
SCott: Accelerating Diffusion Models with Stochastic Consistency Distillation

Hongjian Liu^{*1} Qingsong Xie^{*2} Zhijie Deng³ Chen Chen² Shixiang Tang⁴ Xueyang Fu¹ Zheng-jun Zha¹
Haonan Lu²

Abstract

The iterative sampling procedure employed by diffusion models (DMs) often leads to significant inference latency. To address this, we propose Stochastic Consistency Distillation (SCott) to enable accelerated text-to-image generation, where high-quality generations can be achieved with just 1 – 2 sampling steps, and further improvements can be obtained by adding additional steps. In contrast to vanilla consistency distillation (CD) which distills the ordinary differential equation solvers-based sampling process of a pre-trained teacher model into a student, SCott explores the possibility and validates the efficacy of integrating stochastic differential equation (SDE) solvers into CD to fully unleash the potential of the teacher. SCott is augmented with elaborate strategies to control the noise strength and sampling process of the SDE solver. An adversarial loss is further incorporated to strengthen the consistency constraints in rare sampling steps. Empirically, on the MSCOCO-2017 5K dataset with a Stable Diffusion-V1.5 teacher, SCott achieves an FID (Fréchet Inception Distance) of 22.1, surpassing that (23.4) of the 1-step InstaFlow (Liu et al., 2023) and matching that of 4-step UFOGen (Xu et al., 2023b). Moreover, SCott can yield more diverse samples than other consistency models for high-resolution image generation (Luo et al., 2023a), with up to 16% improvement in a qualified metric.

1. Introduction

Diffusion models (DMs) (Ho et al., 2020; Sohl-Dickstein et al., 2015; Song et al., 2020c) have emerged as a pivotal component in the realm of generative modeling, facilitat-

ing notable progress in domains including image generation (Ramesh et al., 2022; Rombach et al., 2022), video synthesis (Blattmann et al., 2023; Ho et al., 2022), and beyond. In particular, latent diffusion models (LDMs), such as Stable Diffusion (Rombach et al., 2022), have exhibited exceptional capabilities for high-resolution text-to-image synthesis and are acting as fundamental building components for a wide spectrum of downstream applications (Gal et al., 2022; Chen et al., 2023b; Mou et al., 2023).

However, it is widely recognized that DMs’ iterative reverse sampling process leads to slow inference. One remediation is improving the solvers used for discretizing the reverse process (Song et al., 2020a; Lu et al., 2022a;b), but it is still hard for them to generate within a limited number of steps (e.g., 5) due to the inevitable discretization errors. Another strategy involves distilling an ordinary differential equation (ODE) based generation process of a pre-trained DM into a shorter one (Salimans & Ho, 2022; Meng et al., 2023), but the distillation cost is routinely high, and the sample quality degrades compared with the full-step teacher. Alternatively, consistency distillation (CD) trains consistency models (CMs) to fit the consistency mappings characterized by the diffusion ODE for few-step generation (Song et al., 2023), and latent consistency model (LCM) (Luo et al., 2023a) applies CD to the latent space of a pre-trained autoencoder to enable high-resolution image generation, but its sample quality is poor within 1 – 4 sampling steps. Recently, InstaFlow (Liu et al., 2023), UFOGen (Xu et al., 2023b), and ADD (Sauer et al., 2023b) have succeeded in faithfully generating high-resolution images in just 1 – 2 steps, but they share the limitation of failing to trade additional sampling steps for improved outcomes.

The quest for a large-scale text-to-image DM capable of generating high-quality outputs with minimal sampling steps (e.g., 2) while also benefiting from the advantages of additional steps remains an unresolved and crucial challenge. We motivate our solution with observations that CMs enjoy the cost-quality trade-off by alternating denoising and noise injection at inference time, but current CD approaches have not fully unleashed the potential of the teacher, considering that for a well-trained DM, ODE-based solvers usually underperform stochastic differential equation (SDE) ones with adequate sampling steps (Xu et al., 2023a; Karras et al.,

^{*}Equal contribution ¹University of Science and Technology of China ²OPPO AI Center ³Shanghai Jiao Tong University ⁴The Chinese University of Hong Kong. Correspondence to: Qingsong Xie <xieqingsong1@oppo.com>, Zhijie Deng <zhi-jied@sjtu.edu.cn>.

2022; Gonzalez et al., 2023). This is verified by results in Table 1 as well. Empowered by these, we aim to develop a new approach, named **Stochastic Consistency Distillation** (SCott), to combine CD with SDE solvers to accelerate the sampling of high-resolution images from LDMs.

By (Song et al., 2023), CMs are originally defined and learned based on ODE solvers. Naturally, a straightforward adoption of regular SDE solvers suffers from low training stability and poor convergence. To address this, we empirically identify several critical factors that render SCott workable. On one hand, we find it necessary to keep the injected noise in SDE solvers at a moderate intensity to stabilize training while enjoying benefits from the stochasticity inherent in SDE. On the other hand, we find it vital to extend the one-step sampling strategy employed in vanilla CD to a multi-step one to further diminish the discretization errors. The multi-step SDE solver also aids in correcting the accumulated errors in the sampling path, thanks to the injection of random noise (Xu et al., 2023a). With these, we obtain a stronger and more versatile teacher for CD.

We introduce a simple Gaussian formula to the student model and the loss function of CD to accommodate the uncertainty in SDE. Surprisingly, such uncertainty can lead to diverse generations for the distilled student model (see Appendix D.4). From another perspective, the SDE solver implicitly makes stochastic data augmentation for CD, which aids in mode coverage. To mitigate the imperfect consistency constraints provided by L2/ KL loss in CD, an adversarial learning loss is incorporated to correct student output, further boosting the sample quality at 1 – 4 sampling steps. Extensive experiments validate the efficacy of SCott in generating high-quality images with conspicuous details. On MSCOCO-2017 5K validation dataset with a Stable Diffusion-V1.5 (SD1.5) (Rombach et al., 2022) teacher, our 2-step method achieves an FID (Heusel et al., 2017) of 22.1, surpassing the previous state-of-the-art, e.g., 2-step LCM (Luo et al., 2023a) (30.4) and 1 step InstaFlow (Liu et al., 2023) (23.4) and UFOGen (Xu et al., 2023b) (22.5). Besides, SCott can smoothly improve the sample quality with increasing sampling steps. At a 4-step inference, SCott consistently outperforms LCM, InstaFlow, and UFOGen with 1 – 4 steps in terms of both FID and CLIP Score (Heusel et al., 2021). On MJHQ-5K validation dataset with Realistic-Vision-v51 (RV5.1)¹ teacher, 2-step SCott surpasses LCM by a remarkable margin (24.9 v.s. 37.2 in FID, 0.301 v.s. 0.296 in CLIP Score). For the Coverage metric measuring sample diversity (Naeem et al., 2020), 2-step SCott obtains 0.1287 and 0.1778 gains over 2-step LCM on MSCOCO-2017 5K and MJHQ-5K, respectively.

We summarize our contributions as follows:

¹<https://huggingface.co/stablediffusionapi/realistic-vision-v51>.

- We propose SCott, which accelerates diffusion models to generate high-quality outputs within 1 – 4 steps while maintaining the capability for further improvement with additional steps.
- We provide theoretical convergence analysis for SCott and explore crucial factors that render SCott workable. Furthermore, we integrate adversarial learning objectives into SCott to improve the few-step sample quality.
- SCott achieves 1) a state-of-the-art FID score of 22.1 in 2 steps, surpassing competing baselines such as 1-step InstaFlow (23.4) and 2-step LCM (30.4), and matching 4-step UFOGen (22.1), and 2) much higher sample diversity, reflected by the Coverage metric, than LCM (0.9169 v.s. 0.7882).

2. Related Works

2.1. Diffusion Models

Diffusion models (Sohl-Dickstein et al., 2015; Ho et al., 2020; Song et al., 2020c; 2021; Song & Ermon, 2020; Karras et al., 2022; Dhariwal & Nichol, 2021) progressively perturb data to Gaussian noise and are trained to denoise the noise-corrupted data. During inference, diffusion models create samples from Gaussian distribution by reversing the noising process. They have achieved unprecedented success in text-to-image generation (Saharia et al., 2022; Ramesh et al., 2022), image inpainting (Lugmayr et al., 2022), and image editing (Meng et al., 2021; Chen et al., 2023a). To effectively improve the sample quality of conditioned diffusion models, classifier-free guidance (CFG) (Ho & Salimans, 2022) technique is proposed without extra network training.

2.2. Diffusion Acceleration

One of the primary challenges that hinder the practical adoption of diffusion models is the issue of sampling speed due to multiple iterations. Several approaches have been proposed to enhance the sampling efficiency of diffusion models. One type of methods concentrate on training-free numerical solvers (Song et al., 2020b; Lu et al., 2022a;b), such as Denoising Diffusion Implicit Model (DDIM) (Song et al., 2020b) and DPM++ (Lu et al., 2022b). Some researchers explore the approaches of knowledge distillation to compress sampling steps. Progressive Distillation (PD) (Salimans & Ho, 2022) and Classifier-aware Distillation (CAD) (Meng et al., 2023) are designed to reduce sampling steps to below 10 steps via multi-stage distillation. LCM (Luo et al., 2023a) extends CM (Song et al., 2023) to text-to-image generation with few-step inference. However, these methods synthesize blurry samples in four steps. Recently, InstaFlow (Liu et al., 2023), SwiftBrush (Nguyen & Tran, 2023), and DMD (Yin et al., 2024) achieve one-step generation in high-resolution generation faithfully. InstaFlow proposes a one-step sam-



Figure 1. 512×512 resolution images generated by SCott using 2 sampling steps. SCott is trained based on Realistic-Vision-v51.

pling model for text-to-image generation by combining DMs and Rectified Flow (Liu et al., 2022). SwiftBrush adopts variational score distillation (VSD) (Wang et al., 2024) to distill a one-step student. DMD employs distribution matching distillation to enhance the realism of the one-step generator. Nevertheless, they are unable to extend their sampler to multiple steps, and the synthesized images are not satisfactory enough with a single step only. Consistency trajectory models (CTM) (Kim et al., 2023) and Diff-Instruct (Luo et al., 2023b) distill a pre-trained DM into a single-step generator, but their performance on large-scale text-to-image generation is unclear. Motivated by CMs and knowledge distillation, we propose Stochastic Consistency Distillation to generate high-quality images in few-step inference. Our method is able to not only produce high-quality samples with a 2-step sampler but also improve model performance with increasing steps. Furthermore, due to the introduced stochasticity, our method exhibits better sample diversity.

2.3. Diffusion GANs

Denoising Diffusion GAN (DDGAN) (Xiao et al., 2021) first introduces an adversarial objective to model the non-Gaussian distribution of the denoising process with large step sizes. With GANs as a core technique, UFOGen (Xu et al., 2023b) proposes a one-step diffusion GAN for text-to-image generation. However, the image quality can not be significantly improved or even gets worse when increasing sampling steps for UFOGen. Adversarial Diffusion Distillation (Sauer et al., 2023b) distills pre-trained SD models by GANs and score distillation (Poole et al., 2022), achieving one-step generation. However, the training source is not described in the paper, e.g., training time and training data, and hence we can not make a fair comparison with it. Different from UFOGen and ADD which adopt adversarial

learning as their core component, we propose to leverage adversarial loss to strengthen consistency constraints in SCott, producing high-quality images at few-step sampling. Consequently, our method inherits the property of CM which heightens text-to-image alignment and image sharpness with increasing sampling steps, and the image quality is further enhanced by GAN at few-step inference.

3. Preliminary

Let $\mathbf{x} \in \mathbb{R}^k$ denotes a sample from the data distribution $p_{\text{data}}(\mathbf{x})$ and $p(\mathbf{z}_t) = \int p_{\text{data}}(\mathbf{x}) \mathcal{N}(\mathbf{z}_t; \alpha_t \mathbf{x}, \sigma_t^2 \mathbf{I}) d\mathbf{x}, \forall t \in [0, T]$ the marginal distribution specified by the forward diffusion process. α_t and σ_t are positive real-valued functions defining the diffusion schedule so that $p(\mathbf{z}_0) = p_{\text{data}}(\mathbf{x})$ and $p(\mathbf{z}_T) \approx \mathcal{N}(\mathbf{z}_T; \mathbf{0}, \bar{\sigma}^2 \mathbf{I})$ for some $\bar{\sigma}$. A DM $\epsilon_{\theta}(\cdot, t) : \mathbb{R}^k \rightarrow \mathbb{R}^k$ is trained under score matching principles (Vincent, 2011; Song & Ermon, 2019; Ho et al., 2020) for reversing the diffusion process.²

According to the SDE/ODE explanation of the reverse process of DMs (Song et al., 2020c), we can obtain an approximate sample of $p_{\text{data}}(\mathbf{x})$ by drawing a Gaussian noise $\mathbf{z}_T \sim p(\mathbf{z}_T)$ and then invoking a numerical SDE/ODE solver to discretize the reverse process. Let $\hat{\mathbf{z}}_t$ denotes the solution at timestep t , originating from \mathbf{z}_T based on a solver and model $\epsilon_{\theta}(\cdot, t)$, and then $\hat{\mathbf{z}}_0$ represents the sampled data.

3.1. Consistency Distillation

The mentioned solving process usually hinges on tens or hundreds of steps, causing significant inference overheads

²The paper focuses on the ϵ -prediction type of DMs. Other parameterizations are equivalent in theory.

for practical application. A promising solution is to perform consistency distillation (CD) (Song et al., 2023; Song & Dhariwal, 2023) of DMs, yielding a student model $\mathbf{f}_\theta(\cdot, t) : \mathbb{R}^k \rightarrow \mathbb{R}^k$ which enjoys a shortened sampling procedure.

Concretely, CD defines a novel, continuous parameterization of $\mathbf{f}_\theta(\mathbf{z}, t)$ so that $\mathbf{f}_\theta(\mathbf{z}, t) = \mathbf{z}$ when t is tiny, and minimizes the following loss for training

$$\min_{\theta} \mathcal{L}_{CD}(\theta) = \mathbb{E}_{n, z_{t_n}} \left[\lambda(t_n) \left\| \mathbf{f}_\theta(z_{t_n}, t_n) - \mathbf{f}_\theta(\hat{z}_{t_m}, t_m) \right\|_2^2 \right] \quad (1)$$

where $m \in \{1, \dots, n-1\}$ is a hyper-parameter (Song et al., 2023; Luo et al., 2023a), $\lambda(\cdot)$ refers to another positive weighting function, θ^- denotes the exponential moving average (EMA) of θ , and

$$\hat{z}_{t_m} = \frac{\sqrt{\alpha_{t_m}}}{\sqrt{\alpha_{t_n}}} (z_{t_n} - \sqrt{1 - \alpha_{t_n} - \sigma_{t_n}} \cdot \epsilon_\theta(z_{t_n}, t_n)) + \sqrt{1 - \alpha_{t_m}} \cdot \epsilon_\theta(z_{t_n}, t_n) + \sigma_{t_n} \epsilon \quad (2)$$

I.e., \hat{z}_{t_m} represents an intermediate state, starting from z_{t_n} and obtained with the teacher model $\epsilon_\theta(\cdot, t)$ and a one-step DDIM solver (Song et al., 2020b). CD typically sets $\sigma_{t_n} = 0$ to keep \hat{z}_{t_m} and z_{t_n} on the same ODE trajectory.

Although we confine the distance measure in Equation (1) to the squared ℓ_2 distance, the ℓ_1 distance also applies here. We do not consider the Learned Perceptual Image Patch Similarity (LPIPS, Zhang et al., 2018) because it can lead to inflated FID scores (Song & Dhariwal, 2023). The trained \mathbf{f}_θ allows for one-step or multi-step sampling for generating new data (Song et al., 2023).

Limitation. A primary limitation of CD from the viewpoint of distillation is that it has not fully unleashed the potential of the model $\epsilon_\theta(\cdot, t)$: it utilizes one-step DDIM to sample a preceding state of the current one to serve as the teacher for distillation. Yet, for a well-trained DM, ODE-based solvers unusually underperform SDE ones with adequate sampling steps (Gonzalez et al., 2023). Naturally, we ask if we can build an SDE-based teacher for improved CD.

3.2. SDE Solvers for Diffusion Models

The SDE formulation of the reverse-time diffusion process (Song et al., 2020c) takes the form of

$$d\mathbf{x}_t = \underbrace{[f_t \mathbf{x}_t + \frac{g_t^2}{2\sigma_t} \epsilon_\theta(\mathbf{x}_t, t)] dt}_{\text{Probabilistic ODE}} + \underbrace{\frac{g_t^2}{2\sigma_t} \epsilon_\theta(\mathbf{x}_t, t) dt + g_t d\bar{\mathbf{w}}_t}_{\text{Langevin process}} \quad (3)$$

where $\bar{\mathbf{w}}_t$ denotes the standard Wiener process in reverse time, and

$$f_t := \frac{d \log \alpha_t}{dt}, \quad g_t^2 := \frac{d\sigma_t^2}{dt} - 2 \frac{d \log \alpha_t}{dt} \sigma_t^2. \quad (4)$$

Table 1. Performance comparison of typical ODE solvers (DDIM and DPM++) and SDE ones (ER-SDE 5) on MSCOCO-2017 5K with the SD1.5 model. CS denotes CLIP Score to measure text-to-image consistency and CR represents the Coverage metric to assess sample diversity.

SOLVER	STEP	FID ↓	CS ↑	CR ↑
DDIM	50	20.3	0.318	0.9130
DPM++	25	20.3	0.318	0.9118
ER-SDE 5	50	20.2	0.320	0.9172

We can discretize Equation (3) over time to get an approximated solution with various SDE solvers (Gonzalez et al., 2023; Cui et al., 2023; Zhang & Chen, 2022).

Benefits of SDE solvers. According to the theoretical analysis of (Xu et al., 2023a), the divergence between $p(\mathbf{z}_0)$ and the sample distribution $p(\hat{\mathbf{z}}_0)$ stems from the discretization errors along the sampling trajectory and the approximation error between the model and the ground-truth score function (Song et al., 2020c). When the number of function evaluations (NFE) is small, SDE solvers exhibit larger discretization errors than ODE ones— $O(\delta^2)$ v.s. $O(\delta^{\frac{3}{2}})$ with δ as the step size for discretization. On the contrary, the discretization errors become less significant as δ shrinks and the approximation errors dominate, thus SDE solvers achieve higher sample quality than ODE ones thanks to the injection of noise for correcting approximation errors (Kararas et al., 2022).

We validate these arguments with results in Table 1, where the ER-SDE 5 solver (Cui et al., 2023) outperforms ODE solvers DDIM and DPM++ (Lu et al., 2022b) in terms of both sample quality and diversity with 50 sampling steps. Besides, the noise injected in SDE solvers implicitly makes stochastic data augmentation for CD. With such observations, we are motivated to explore the possibility of combining SDE solvers and CD, aiming at acquiring stronger teachers for CD.

4. Methodology

Our goal is to generate high-quality samples within a few-step inference while maintaining the trade-off to improve sample quality with additional sampling steps. Previous methods are either failed to generate high-quality samples within 1 – 4 steps (Lu et al., 2022a; Luo et al., 2023a; Salimans & Ho, 2022) or unable to trade additional sampling steps for improved outcomes (Liu et al., 2023; Xu et al., 2023b; Sauer et al., 2023b). We observe that CMs enjoy the trade-off by alternating denoising and noise injection at inference time. However, CD approaches haven’t unleashed the potential power of the pre-trained teacher DMs, considering ODE solvers underperform SDE ones when the NFE is large. We first lay out a justification for the feasibility of

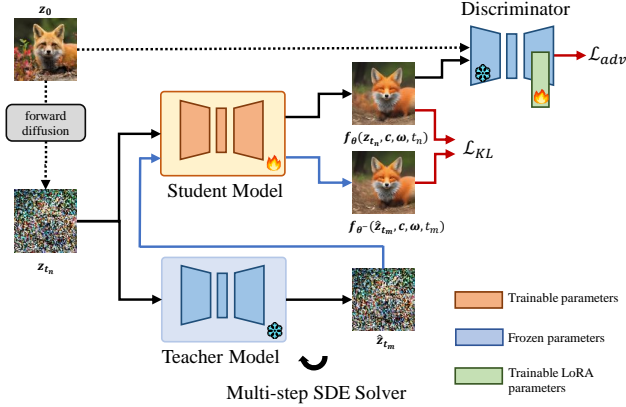


Figure 2. Overview of SCott. SCott distills a pre-trained teacher DM into a student one for accelerated sampling. Compared to the vanilla consistency distillation approach, we introduce a multi-step SDE solver to establish a stronger and more versatile teacher. We refine the student model to yield a Gaussian distribution to account for the uncertainty in SDE solving. We also include an adversarial learning loss to boost the sample quality with rare sampling steps. Note that we omit the EMA module for brevity.

combining CD with SDE solvers. Then, we identify several critical factors to make SCott workable for high-resolution text-to-image generation. We also introduce GAN loss to further enhance the sampling quality at rare steps. Our method is summarized in Figure 2.

4.1. Justification of Using SDE Solvers for CD

Despite our motivation for combining SDE solvers and CD being sensible from the perspective of model distillation, a major concern arises as to whether it is reasonable to do so because CD is originally defined on ODE trajectories. In this section, we provide both theoretical justification and empirical investigation on this.

Theoretical justification of using SDE solvers for CD. Following (Song et al., 2023), we provide the convergence proof of using SDE solvers in CD.

Theorem 4.1. *Let $\Delta t := \max_{n \in [1, N]} |t_{n+1} - t_n|$ where $t \in [\epsilon, T]$. Assume $f_\theta(\cdot, \cdot)$ is Lipschitz in x with constant L_1 . Denote $f(\cdot, \cdot)$ the consistency function of the SDE defined in Equation (3). Assume the SDE solver Φ_{SDE} has a local error bound of $O((\Delta t)^{p+1})$ with $p \geq 1$. Then, if we have $\mathcal{L}_{KL}^N(\theta, \Phi_{SDE}) = 0$, we have*

$$\sup_{n, x} \|f_\theta(x_{t_n}, t_n) - f(x_{t_n}, t_n)\|_2 = O((\Delta t)^p).$$

Proof. We refer to Theorem A.1 for the full proof. \square

Empirical investigation of using SDE solvers for CD. Specifically, we experiment on a simple 1D task—characterizing a Gaussian mixture distribution with 3 uniform components $p_{\text{data}}(x) := \frac{1}{3}\mathcal{N}(x; -1.5, 0.2^2\mathbf{I}) +$

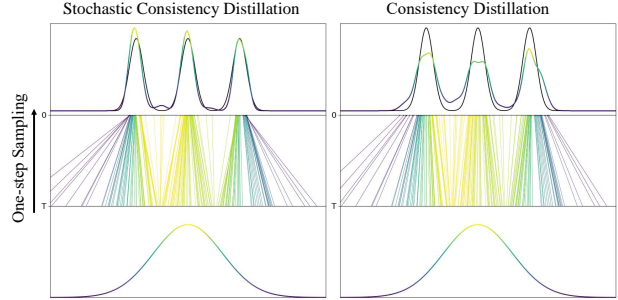


Figure 3. Comparison of stochastic CD (based on SDE solvers) and vanilla CD (based on ODE solvers) on a synthetic generation task. The other experimental settings for the two cases are identical.

$\frac{1}{3}\mathcal{N}(x; 0, 0.2^2\mathbf{I}) + \frac{1}{3}\mathcal{N}(x; 1.5, 0.2^2\mathbf{I})$. We first train a DM, instantiated as a 4-layer MLP, with a standard Gaussian prior on it, and then perform CD based on Equation (1) with SDE and ODE solvers respectively. In particular, we select the EDM solver (Karras et al., 2022) with the noise coefficient equaling 0 as the ODE solver and the EDM solver with that equaling 2 as the SDE solver.

We plot the one-step sampling results of the trained models in Figure 3, where the Gaussian noise and sampling trajectory are also displayed. As shown, the stochastic CD can successfully map noise points to suitable target samples, even with higher accuracy than the vanilla CD. One possible explanation for this phenomenon is that, for a given t_m , the sampled states from the SDE solver are likely to surround the deterministic states sampled from the ODE solver. This situation can be viewed as a form of data augmentation, which helps the student model better align and rectify its predictions. These results provide concrete evidence that we can indeed use SDE solvers for CD.

4.2. Stochastic Consistency Distillation (SCott)

For large-scale modeling on high-resolution natural images, we, however, observe that directly utilizing an SDE solver for CD leads to training instability and poor convergence. We address this issue by introducing multiple crucial modifications to straightforward implementations.

Controlling the level of noise in SDE solvers. It is a natural idea to control the level of random noise injected in SDE solvers to stabilize training. Taking the DDIM solver in Equation (2) for example, the σ_{t_n} controls the intensity of injected noise and typically we can introduce a coefficient η for scaling it (Song et al., 2020a):

$$\sigma_{t_n}(\eta) := \eta \sqrt{(1 - \alpha_{t_{n-1}})/(1 - \alpha_{t_n})} \sqrt{1 - \alpha_{t_n}/\alpha_{t_{n-1}}}. \quad (5)$$

Increasing η from 0 to a positive value results in a set of SDE solvers with increasingly intensive noise, starting from an ODE one. We empirically experiment with the solvers for SCott and present the results in Table 5. As shown, we

indeed need to select a reasonable noise level to enjoy the benefits of SDE solvers for error correction while avoiding introducing excessive variance. Following this insight, we include the more advanced ER-SDE solver (Cui et al., 2023) to SCott. The novel noise scaling function in the ER-SDE solver also provides a simple way to control the intensity of noise, which aligns with our requirements for SDE solvers.

Multi-step sampling. The discretization errors of SDE solvers are larger than those of ODE solvers (Xu et al., 2023a). A simple remediation to this is to decrease the step size, but doing so leads to slow convergence and degraded results for SCott, consistent with the results in (Luo et al., 2023a). To address this, we propose a multi-step sampling strategy for SCott. Specifically, for a sample z_{t_n} at the time t_n on the SDE trajectory, to obtain the estimated state \hat{z}_{t_m} for a preceding timestep t_m , we split the time interval $t_n - t_m$ into h intervals, namely, sampling with a step size of $\frac{t_n - t_m}{h}$, as illustrated in Figure 4. We denote the solution as $\hat{z}_{t_m} = \Phi_{SDE}(\epsilon_\theta, z_{t_n}, t_n, t_m, h)$.

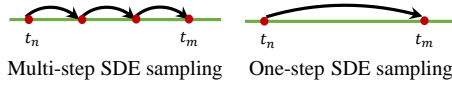


Figure 4. Multi-step SDE solver sampling

Through multi-step sampling, we can reduce the discretization errors in SDE solvers as the interval shrinks. Besides, the multi-step SDE solver aids in correcting the accumulated errors in the sampling path with the injection of random noise. Empirically, we set $t_m = t_n - 24$ and $h = 3$.

A Gaussian student and the parameterization. To accommodate the uncertainty in stochastic consistency distillation, we introduce a Gaussian formula to the student model and CD objective. For z_{t_n} , we predict both the Gaussian mean and variance of the sample. Specifically, we reparameterize our network f_θ to produce $[\mu_{t_n}, \sigma_{t_n}^2] = f_\theta(z_{t_n}, c, \omega, t_n)$ where we also incorporate the condition c and the classifier-free guidance (CFG) (Ho & Salimans, 2022) scale ω as model input. In practice, we only double the output channels of the final layer of the model to fulfill the need to produce both the mean and variance. Then, we extend the original ℓ_2 loss for CD as the Kullback–Leibler (KL) divergence between Gaussians:

$$\mathcal{L}_{\mathcal{KL}}(\theta, \theta^-; \Phi_{SDE}) := \mathbb{E}_{t_n, z_{t_n}} \left[\lambda(t_n) D_{\text{KL}}(\mathcal{N}(\mu_{t_n}, \sigma_{t_n}^2) \parallel \mathcal{N}(\hat{\mu}_{t_m}, \hat{\sigma}_{t_m}^2)) \right] \quad (6)$$

where $[\hat{\mu}_{t_m}, \hat{\sigma}_{t_m}^2] = f_{\theta^-}(\hat{z}_{t_m}, c, \omega, t_m)$. Gaussian formulation allows for a more reliable representation of the consistency target, capturing not only its expectation but also

Algorithm 1 Stochastic Consistency Distillation

Input: dataset \mathcal{D} , initial consistency model parameter θ , discriminator parameter ϕ , SDE solver Φ_{SDE} , encoder $E(\cdot)$, noise schedule α_t, σ_t , sampling steps h , adversarial loss $\mathcal{L}_{adv}(\cdot, \cdot)$, weight $\lambda(\cdot)$, CFG scale ω , EMA rate μ , loss coefficient λ_{adv}

$\theta^- \leftarrow \theta$

repeat

 Sample $(x_0, c) \sim \mathcal{D}$

 Sample $z_{t_n} \sim \mathcal{N}(\alpha_{t_n} E(x_0), \sigma_{t_n}^2 \mathbf{I})$

$\hat{z}_{t_m} \leftarrow \Phi_{SDE}(\epsilon_\theta, z_{t_n}, t_n, t_m, h)$

 Calculate $\mathcal{L}_{\mathcal{KL}}(\theta, \theta^-; \Phi_{SDE})$ with Equation (6)

 Calculate $\mathcal{L}_{adv}(\theta, \phi)$ with Equation (7)

 Calculate $\mathcal{L}_{SCott}(\theta, \phi)$ with Equation (8)

$\theta \leftarrow \theta - \frac{\partial}{\partial \theta} \mathcal{L}_{SCott}(\theta, \phi)$

$\phi \leftarrow \phi - \frac{\partial}{\partial \phi} \mathcal{L}_{SCott}(\theta, \phi)$

$\theta^- \leftarrow \text{stop_grad}(\mu\theta^- + (1 - \mu)\theta)$

until convergence

the uncertainty. We observe that such uncertainty can lead to an increase in diversity among generated samples.

Introducing GAN into SCott. For high-resolution text-to-image generation, considering the high data dimensionality and complex data distribution, simply using L2 or KL loss fails to capture data discrepancy precisely, thus providing imperfect consistency constraints. Suggested by CTM (Kim et al., 2023) which leverages GAN to improve trajectory estimation in the process of distillation, we integrate GAN into SCott to mitigate the restriction of KL loss. However, it is non-trivial to directly employ CTM’s GAN. Firstly, CTM’s GAN performs on the pixel level while SCott performs on the latent space. For high-resolution image generation, employing a GAN that operates directly on pixel values would significantly increase the training cost. Secondly, SCott is designed to accelerate text-to-image tasks, the interaction between textual information and visual representation is not considered in the design of CTM’s GAN. To address these issues, we design a low-rank adaptation (LoRA) (Hu et al., 2021) discriminator with time and text projection, which renders adversarial training successfully in SCott.

LoRA discriminator. To accelerate training, the discriminator is initialized by pre-trained U-Net in SD (Rombach et al., 2022). However, we find training the whole U-Net is expensive and unstable. Therefore, we freeze the encoder of the U-Net and only train the LoRA parameters of the decoder of the network. The frozen encoder of the U-Net extracts rich latent representations from the input and conditions, while the LoRA decoder acts as discriminator heads to distinguish between real images and generated images. By employing this approach, only 3.64% of the parameters in the U-Net are updated, which not only contributes to computational efficiency but also increases the overall stability of the adversarial training.

Table 2. Comparisons with the state-of-the-art methods on MSCOCO-2017 5K in terms of FID, CS, CR. All models are based on SD1.5.

METHOD	REFERENCES	STEP	TIME (S)	FID ↓	CS ↑	CR ↑
DPM++ (LU ET AL., 2022B)	ARXIV (2022)	25	0.88	20.1	0.318	0.9118
DDIM (SONG ET AL., 2020B)	ICLR (2021)	50	–	20.3	0.318	0.9130
PD (SALIMANS & HO, 2022)	ICLR (2022)	4	0.21	26.4	0.300	–
CAD (MENG ET AL., 2023)	CVPR (2023)	8	0.34	24.2	0.300	–
LCM (LUO ET AL., 2023A)	ARXIV (2023)	2	0.13	30.4	0.293	0.7882
INSTAFLOW-0.9B (LIU ET AL., 2023)	ICLR (2024)	1	0.09	23.4	0.304	–
INSTAFLOW-1.7B (LIU ET AL., 2023)	ICLR (2024)	1	0.12	22.4	0.309	–
UFOGEN (XU ET AL., 2023B)	CVPR (2024)	1	0.09	22.5	0.311	–
UFOGEN (XU ET AL., 2023B)	CVPR (2024)	4	–	22.1	0.307	–
SCOTT (OURS)		1	0.09	26.5	0.295	0.8442
SCOTT (OURS)		2	0.13	22.1	0.309	0.9169
SCOTT (OURS)		4	0.21	21.9	0.312	0.9210

Conditional discriminator. Since SCott predicts the clean image \hat{z}_0 , we can directly perform adversarial learning between real image z_0 and generated image \hat{z}_0 . However, we find such a naive design makes training unstable for text-to-image tasks. To surmount this challenge, the timestep t_n and text c are propagated into the discriminator as conditions.

Following (Sauer et al., 2023a), we train our discriminator D_ϕ with hinge loss:

$$\begin{aligned} \mathcal{L}_{adv}(\theta, \phi) = & \mathbb{E}_{z_0, c} \left[\max(0, 1 - D_\phi(z_0, c, 0)) \right] \\ & + \mathbb{E}_{z_{t_n}, c, t_n} \left[\max(0, 1 + D_\phi(\bar{f}_\theta(z_{t_n}, c, \omega, t_n), c, t_n)) \right], \end{aligned} \tag{7}$$

where \bar{f}_θ denotes the function that produces the Gaussian mean within the model f_θ .

Overall, SCott is trained with the following objective:

$$\mathcal{L}_{SCott}(\theta, \phi) = \mathcal{L}_{\mathcal{KL}}(\theta, \theta^-; \Phi_{SDE}) + \lambda_{adv} \mathcal{L}_{adv}(\theta, \phi). \tag{8}$$

In practice, we set $\lambda_{adv} = 0.4$ to control the strength of the discriminator for refining the outputs of f_θ . To save GPU memory, the training is performed in latent space. We find the introducing of GAN loss renders SCott to produce more realistic outputs, particularly at rare steps. We present the pseudo-code for SCott in Algorithm 1.

5. Experiments

In this section, we elaborate on the experimental results of our proposed SCott model for the text-to-image generation task. We start with the comparison with other works in Section 5.1, and then ablate components of SCott in Section 5.2, highlighting the effectiveness of our proposed components.

5.1. Comparison with Other Methods

Comparison on MSCOCO-2017 5K with SD1.5. To kick-start the comparisons with the state-of-the-art methods, we evaluate the MSCOCO-2017 5K validation dataset (Lin et al., 2014). Zero-shot FID and CLIP Score (CS) with ViT-g/14 backbone (Radford et al., 2021) are exploited as objective metrics. To measure diversity, Coverage (CR) (Naeem et al., 2020) is used as another metric. Table 2 summarizes the performance of our SCott and comparative methods consisting of PD (Salimans & Ho, 2022), CAD (Meng et al., 2023), LCM (Luo et al., 2023a), InstaFlow (Liu et al., 2023), UFOGen (Xu et al., 2023b). Since PD (Salimans & Ho, 2022), CAD (Meng et al., 2023), InstaFlow (Liu et al., 2023), and UFOGen (Xu et al., 2023b) do not list CR value, we leave them –. Time denotes inference time on a single A100. LCM is implemented according to the official in our setting.

Among all the methods, our 2-step Scott presents superior FID and CS values than 4-step PD (Salimans & Ho, 2022), 8-step CAD (Meng et al., 2023) 1 step InstaFlow-0.9B (Liu et al., 2023), 2-step LCM (Luo et al., 2023a). It is impressive to see that our 2-step SCott beats InstaFlow-1.7B which doubles the parameter size. These results demonstrate our SCott significantly enhances the quality of the generated images while reducing inference steps. The improvements lie in that the proposed $\mathcal{L}_{\mathcal{KL}}$ in SCott is able to remarkably reduce the sampling steps and adversarial loss further improves image quality. Interestingly, the CS decreases by 0.004 when the inference step increases from 1 to 4 for UFOGen (Xu et al., 2023b). Meanwhile, by changing the inference step from 1 to 4, all the metrics are improved for our SCott, and 4-step Scott also outperforms 4-step UFOGen regarding both FID and CS. The result indicates the improvement is limited for UFOGen when increasing sampling steps while our method is much more powerful in

Table 3. Comparisons with the state-of-the-art methods on MSCOCO-2014 30K in terms of FID. All models are based on SD1.5.

METHOD	STEP	FID ↓
SWIFTBRUSH (NGUYEN & TRAN, 2023)	1	16.67
UFOGEN (XU ET AL., 2023B)	1	12.78
INSTAFLOW-0.9B (XU ET AL., 2023B)	1	13.10
DMD (YIN ET AL., 2024)	1	11.49
SCOTT (OURS)	2	12.22
SCOTT (OURS)	4	11.09

Table 4. Comparisons with the state-of-the-art methods on MJHQ-5K in terms of FID, CS, CR. All models are based on RV5.1.

METHOD	STEP	TIME (S)	FID ↓	CS ↑	CR ↑
DPM++ (LU ET AL., 2022B)	25	0.88	22.1	0.320	0.8664
DDIM (SONG ET AL., 2020B)	50	—	22.9	0.320	0.8536
LCM (LUO ET AL., 2023A)	2	0.13	37.2	0.296	0.7016
SCOTT (OURS)	2	0.13	24.9	0.301	0.8794

enhancing image quality with increasing steps, which is meaningful in the scenarios requiring high-quality images with more affordable computational budgets. The proposed SCott obtains higher CR than LCM (Luo et al., 2023a), and even outperforms the ODE solvers, 25-step DPM++ (Lu et al., 2022b) and 50-step DDIM (Song et al., 2020b), indicating our SCott successfully increases diversity due to the introduced randomness.

Appendix D.1 presents the qualitative comparisons involving InstaFlow and LCM. Notably, 2-step SCott gains significant improvements over 2-step LCM and 1-step InstaFlow in terms of image quality and text-to-image alignment. We also observe that our generated images exhibit sharper textures and finer details, compared to the images generated by InstaFlow and LCM.

Comparison on MSCOCO-2014 30K with SD1.5. For complete comparisons, we also extend our evaluation on MSCOCO-2014 30K (Lin et al., 2014). We benchmark our method against DMD, SwiftBrush and UFOGen. The result is presented in Table 3. We have observed that 2-step SCott surpasses the UFOGEN, SwiftBrush, and InstaFlow, comparable to DMD. It’s worth noting that DMD can only generate samples using a single step, whereas our method offers the capability to enhance the quality of the generated samples with additional steps. These results validate the effectiveness of our approach in achieving higher-quality samples within 2 steps and progressively improving performance by leveraging additional inference steps.

Comparison on MJHQ-5K with RV5.1. To better assess the quality of produced images, we further conduct experi-

ments on MJHQ-5K, randomly selected from MJHQ-30K³, since it owns high image quality and high image-text alignment, and the correlation between human preference and FID score on the MJHQ is verified by user study. The evaluation metrics of several methods with RV5.1 as a teacher are listed in Table 4. The reason for distilling RV5.1 is that RV5.1 is much stronger than SD1.5 for text-to-image consistency, which can be found in Table 11. LCM is also implemented according to the official code. Since the training codes of PD, CAD, InstaFlow, and UFOGen are unavailable, the metrics of these methods are not included. The result again presents our SCott outperforms LCM (Luo et al., 2023a) by a large margin, because our SDE-based CD provides a stronger and more versatile teacher than ODE-based CD in LCM, and the student output is further refined to be real data by the proposed discriminator.

5.2. Ablation Study

To analyze the key components of our method, we make a thorough ablation study to verify the effectiveness of the proposed SCott.

SDE solver. Table 5 depicts the results using deterministic and stochastic solvers for CD. DDIM(η) represents DDIM solver with noise coefficient η , where η denotes the hyperparameter that controls the strength of random noise injected in Eq.2. η achieves an interpolation between the deterministic DDIM ($\eta = 0$) and original DDPM ($\eta = 1$). As observed in Table 5, the SDE-based DDIM ($\eta = 0.1, 0.2$) surpasses ODE-based DDIM ($\eta = 0$) for CD, demonstrating the superiority of SDE solver for CD. This is because the injection of noise at moderate intensity in SDE solvers aids in correcting estimated errors of the teacher model with multiple sampling steps, leading to a more powerful teacher. However, excessive noise intensity leads to poor convergence and degraded samples, as shown in DDIM($\eta = 0.6$). These results indicate it is crucial to control the noise strength in SCott since large noise leads to low training stability. The 2-order ER-SDE 5 solver further enhances the performance, this is because 1. the 2-order ER-SDE 5 exhibits smaller discretization errors compared to the 1-order DDIM solver. 2. the noise function in ER-SDE 5 mitigates excessive noise, which leads to good convergence. Table 8 shows that SCott without GAN also surpasses the ODE solver-based LCM, further illustrating the benefits of using SDE solvers for CD.

Multi-step SDE solver sampling. As outlined in Table 6, we study the sampling steps in the process of estimating \hat{z}_{t_m} given z_{t_n} . The results indicate that multi-step SDE solvers are superior to single-step solvers. The reason is that SDE solvers usually require multiple iterations to reach the correct destination, demonstrating the choice of SDE solver steps during CD is critical to make SCott successful.

³<https://huggingface.co/playgroundai/playground-v2-1024px-aesthetic>.

Table 5. The performance comparison of different solvers on MJHQ-5K with 2-step inference. All models are based on RV5.1.

SDE SOLVER	FID ↓	CS ↑	CR ↑
DDIM($\eta = 0$)	27.4	0.296	0.8450
DDIM($\eta = 0.1$)	26.2	0.297	0.8713
DDIM($\eta = 0.2$)	25.2	0.299	0.8786
DDIM($\eta = 0.3$)	27.7	0.298	0.8717
DDIM($\eta = 0.6$)	29.7	0.298	0.8162
ER-SDE 5	24.9	0.301	0.8794

Table 6. The performance comparison of SDE solver steps with 2-step inference on MJHQ-5K. All models are based on RV5.1.

SOLVER STEP	FID ↓	CS ↑	CR ↑
1	27.4	0.299	0.8461
2	25.4	0.300	0.8724
3	24.9	0.301	0.8794

Gaussian Formula. We conduct an ablation study of the Gaussian formula Table 7. The results depicted in Table 7 demonstrate the effectiveness of our proposed Gaussian formula and KL loss. Compared to the L2 loss, Gaussian parameterization and KL loss reduce FID by 0.3 and improve CR by 0.0072. The injection of noise in SDE solvers introduces additional randomness in CD, which can not be effectively captured by the L2 loss. To address this issue, we leverage the Gaussian formulation and KL loss to the consistency target, enabling a better adaption to the randomness.

Table 7. The performance comparison of Gaussian formula and KL loss on MJHQ-5K with backbone RV5.1.

LOSS	STEP	FID ↓	CS ↑	CR ↑
L2	4	25.0	0.304	0.8766
GS+KL	4	24.7	0.304	0.8838

Discriminator. Table 8 illustrates our discriminator leads to gains with respect to FID, CS and CR using different inference steps. We observe our LoRA discriminator achieves better sample qualities than the fully parameterized one. Compared with the discriminator without condition, SCott leverages both the time and text conditions. Such a design helps the discriminator better distinguish between real and generated samples. Interestingly, we observe that our discriminator can also improve the outputs of LCM, which indicates the generalization capability of our discriminator.

Inference steps. As a CM, SCott can improve sample quality as NFE increases. We provide both qualitative and quantitative results of SCott across different inference steps. Table 9 demonstrates SCott consistently improves sample

Table 8. The performance comparison of Discriminator on MSCOCO-2017 5k with backbone SD 1.5.

LOSS	STEP	FID ↓	CS ↑	CR ↑
SCOTT (Without GAN)	2	25.0	0.300	0.867
LCM	2	30.4	0.293	0.788
LCM + GAN	2	29.2	0.297	0.8160
SCOTT (Full Discriminator)	2	23.5	0.302	0.8880
SCOTT (Without Condition)	2	26.1	0.297	0.8412
SCOTT	2	22.1	0.309	0.9169

Table 9. Performance comparison of our Scott on MJHQ-5K with different inference steps with backbone RV5.1.

STEP	FID ↓	CS ↑	CR ↑
1	29.0	0.290	0.8226
2	24.9	0.301	0.8794
3	24.8	0.303	0.8804
4	24.7	0.304	0.8838

quality as NFE increases, including FID, CS, and CR, which benefit from the capability of CMs. Visual results of SCott at inference steps 2, 4, and 8 are shown in Figure 11. The seeds are the same within the columns. SCott can already generate high-quality samples with 2-step inference. With additional steps, SCott can consistently refine the details of the samples. Therefore, SCott achieves a trade-off between computational resources and quality.

6. Conclusions

In this paper, we propose stochastic consistency distillation (SCott), a novel approach for accelerating text-to-image diffusion models. SCott integrates SDE solvers into consistency distillation to unleash the potential of the teacher, implemented by controlling noise strength and sampling step of SDE solvers. Adversarial learning is further utilized to aid SCott in generating high-quality images in rare-step sampling. SCott is capable of yielding high-quality images with 2 steps only, surpassing 2-step LCM and 1-step InstaFlow, comparable to 4-step UFOGen. Additionally, SCott consistently improves performance with increasing steps and exhibits higher diversity than competing baselines.

Impact Statement

There are many potential societal consequences of our work. Like other generative models, DPMs can be employed to generate misleading or harmful content, and our proposed method may further amplify the negative impact of generative AI for malicious purposes.

References

- Betzalel, E., Penso, C., Navon, A., and Fetaya, E. A study on the evaluation of generative models. *arXiv preprint arXiv:2206.10935*, 2022.
- Blattmann, A., Rombach, R., Ling, H., Dockhorn, T., Kim, S. W., Fidler, S., and Kreis, K. Align your latents: High-resolution video synthesis with latent diffusion models. In *Proceedings of the IEEE/CVF Conference on Computer Vision and Pattern Recognition*, pp. 22563–22575, 2023.
- Chen, J., Pan, Y., Yao, T., and Mei, T. Controlstyle: Text-driven stylized image generation using diffusion priors. In *Proceedings of the 31st ACM International Conference on Multimedia*, pp. 7540–7548, 2023a.
- Chen, W., Hu, H., Li, Y., Rui, N., Jia, X., Chang, M.-W., and Cohen, W. W. Subject-driven text-to-image generation via apprenticeship learning. *arXiv preprint arXiv:2304.00186*, 2023b.
- Cui, Q., Zhang, X., Lu, Z., and Liao, Q. Elucidating the solution space of extended reverse-time sde for diffusion models, 2023.
- Dhariwal, P. and Nichol, A. Diffusion models beat gans on image synthesis. *Advances in neural information processing systems*, 34:8780–8794, 2021.
- Gal, R., Alaluf, Y., Atzmon, Y., Patashnik, O., Bermano, A. H., Chechik, G., and Cohen-Or, D. An image is worth one word: Personalizing text-to-image generation using textual inversion. *arXiv preprint arXiv:2208.01618*, 2022.
- Gonzalez, M., Fernandez, N., Tran, T., Gherbi, E., Hajri, H., and Masmoudi, N. Seeds: Exponential sde solvers for fast high-quality sampling from diffusion models, 2023.
- Hessel, J., Holtzman, A., Forbes, M., Bras, R. L., and Choi, Y. CLIPScore: a reference-free evaluation metric for image captioning. In *EMNLP*, 2021.
- Heusel, M., Ramsauer, H., Unterthiner, T., Nessler, B., and Hochreiter, S. Gans trained by a two time-scale update rule converge to a local nash equilibrium. *Advances in neural information processing systems*, 30, 2017.
- Ho, J. and Salimans, T. Classifier-free diffusion guidance. *arXiv preprint arXiv:2207.12598*, 2022.
- Ho, J., Jain, A., and Abbeel, P. Denoising diffusion probabilistic models. *Advances in neural information processing systems*, 33:6840–6851, 2020.
- Ho, J., Chan, W., Saharia, C., Whang, J., Gao, R., Gritsenko, A., Kingma, D. P., Poole, B., Norouzi, M., Fleet, D. J., et al. Imagen video: High definition video generation with diffusion models. *arXiv preprint arXiv:2210.02303*, 2022.
- Hu, E. J., Wallis, P., Allen-Zhu, Z., Li, Y., Wang, S., Wang, L., Chen, W., et al. Lora: Low-rank adaptation of large language models. In *International Conference on Learning Representations*, 2021.
- Karras, T., Aittala, M., Aila, T., and Laine, S. Elucidating the design space of diffusion-based generative models. *Advances in Neural Information Processing Systems*, 35: 26565–26577, 2022.
- Kim, D., Lai, C.-H., Liao, W.-H., Murata, N., Takida, Y., Uesaka, T., He, Y., Mitsufuji, Y., and Ermon, S. Consistency trajectory models: Learning probability flow ode trajectory of diffusion. *arXiv preprint arXiv:2310.02279*, 2023.
- Langley, P. Crafting papers on machine learning. In Langley, P. (ed.), *Proceedings of the 17th International Conference on Machine Learning (ICML 2000)*, pp. 1207–1216, Stanford, CA, 2000. Morgan Kaufmann.
- Lin, T.-Y., Maire, M., Belongie, S., Hays, J., Perona, P., Ramanan, D., Dollár, P., and Zitnick, C. L. Microsoft coco: Common objects in context. In *Computer Vision—ECCV 2014: 13th European Conference, Zurich, Switzerland, September 6–12, 2014, Proceedings, Part V 13*, pp. 740–755. Springer, 2014.
- Liu, X., Gong, C., and Liu, Q. Flow straight and fast: Learning to generate and transfer data with rectified flow. *arXiv preprint arXiv:2209.03003*, 2022.
- Liu, X., Zhang, X., Ma, J., Peng, J., and Liu, Q. InstafLOW: One step is enough for high-quality diffusion-based text-to-image generation. *arXiv preprint arXiv:2309.06380*, 2023.
- Lu, C., Zhou, Y., Bao, F., Chen, J., Li, C., and Zhu, J. Dpm-solver: A fast ode solver for diffusion probabilistic model sampling in around 10 steps. *Advances in Neural Information Processing Systems*, 35:5775–5787, 2022a.
- Lu, C., Zhou, Y., Bao, F., Chen, J., Li, C., and Zhu, J. Dpm-solver++: Fast solver for guided sampling of diffusion probabilistic models. *arXiv preprint arXiv:2211.01095*, 2022b.

- Lugmayr, A., Danelljan, M., Romero, A., Yu, F., Timofte, R., and Van Gool, L. Repaint: Inpainting using denoising diffusion probabilistic models. In *Proceedings of the IEEE/CVF Conference on Computer Vision and Pattern Recognition*, pp. 11461–11471, 2022.
- Luo, S., Tan, Y., Huang, L., Li, J., and Zhao, H. Latent consistency models: Synthesizing high-resolution images with few-step inference. *arXiv preprint arXiv:2310.04378*, 2023a.
- Luo, W., Hu, T., Zhang, S., Sun, J., Li, Z., and Zhang, Z. Diff-instruct: A universal approach for transferring knowledge from pre-trained diffusion models. *arXiv preprint arXiv:2305.18455*, 2023b.
- Meng, C., He, Y., Song, Y., Song, J., Wu, J., Zhu, J.-Y., and Ermon, S. Sdedit: Guided image synthesis and editing with stochastic differential equations. In *International Conference on Learning Representations*, 2021.
- Meng, C., Rombach, R., Gao, R., Kingma, D., Ermon, S., Ho, J., and Salimans, T. On distillation of guided diffusion models. In *Proceedings of the IEEE/CVF Conference on Computer Vision and Pattern Recognition*, pp. 14297–14306, 2023.
- Mou, C., Wang, X., Xie, L., Zhang, J., Qi, Z., Shan, Y., and Qie, X. T2i-adapter: Learning adapters to dig out more controllable ability for text-to-image diffusion models. *arXiv preprint arXiv:2302.08453*, 2023.
- Naeem, M. F., Oh, S. J., Uh, Y., Choi, Y., and Yoo, J. Reliable fidelity and diversity metrics for generative models. In *37th International Conference on Machine Learning, ICML 2020*, pp. 7133–7142. International Machine Learning Society (IMLS), 2020.
- Nguyen, T. H. and Tran, A. Swiftbrush: One-step text-to-image diffusion model with variational score distillation. *arXiv preprint arXiv:2312.05239*, 2023.
- Podell, D., English, Z., Lacey, K., Blattmann, A., Dockhorn, T., Müller, J., Penna, J., and Rombach, R. Sdxl: Improving latent diffusion models for high-resolution image synthesis. *arXiv preprint arXiv:2307.01952*, 2023.
- Poole, B., Jain, A., Barron, J. T., and Mildenhall, B. Dreamfusion: Text-to-3d using 2d diffusion. In *The Eleventh International Conference on Learning Representations*, 2022.
- Radford, A., Kim, J. W., Hallacy, C., Ramesh, A., Goh, G., Agarwal, S., Sastry, G., Askell, A., Mishkin, P., Clark, J., et al. Learning transferable visual models from natural language supervision. In *International conference on machine learning*, pp. 8748–8763. PMLR, 2021.
- Ramesh, A., Dhariwal, P., Nichol, A., Chu, C., and Chen, M. Hierarchical text-conditional image generation with clip latents. *arXiv preprint arXiv:2204.06125*, 1(2):3, 2022.
- Rombach, R., Blattmann, A., Lorenz, D., Esser, P., and Ommer, B. High-resolution image synthesis with latent diffusion models. In *Proceedings of the IEEE/CVF conference on computer vision and pattern recognition*, pp. 10684–10695, 2022.
- Saharia, C., Chan, W., Saxena, S., Li, L., Whang, J., Denton, E. L., Ghasemipour, K., Gontijo Lopes, R., Karagol Ayan, B., Salimans, T., et al. Photorealistic text-to-image diffusion models with deep language understanding. *Advances in Neural Information Processing Systems*, 35: 36479–36494, 2022.
- Salimans, T. and Ho, J. Progressive distillation for fast sampling of diffusion models. In *International Conference on Learning Representations*, 2022. URL <https://openreview.net/forum?id=TiDIXIpzhoI>.
- Sauer, A., Karras, T., Laine, S., Geiger, A., and Aila, T. Stylegan-t: Unlocking the power of gans for fast large-scale text-to-image synthesis. In *International Conference on Machine Learning*, 2023a.
- Sauer, A., Lorenz, D., Blattmann, A., and Rombach, R. Adversarial diffusion distillation. *arXiv preprint arXiv:2311.17042*, 2023b.
- Schuhmann, C., Beaumont, R., Vencu, R., Gordon, C., Wightman, R., Cherti, M., Coombes, T., Katta, A., Mullis, C., Wortsman, M., et al. Laion-5b: An open large-scale dataset for training next generation image-text models. *Advances in Neural Information Processing Systems*, 35: 25278–25294, 2022.
- Sohl-Dickstein, J., Weiss, E., Maheswaranathan, N., and Ganguli, S. Deep unsupervised learning using nonequilibrium thermodynamics. In *International conference on machine learning*, pp. 2256–2265. PMLR, 2015.
- Song, J., Meng, C., and Ermon, S. Denoising diffusion implicit models. In *International Conference on Learning Representations*, 2020a.
- Song, J., Meng, C., and Ermon, S. Denoising diffusion implicit models. *arXiv preprint arXiv:2010.02502*, 2020b.
- Song, Y. and Dhariwal, P. Improved techniques for training consistency models. *arXiv preprint arXiv:2310.14189*, 2023.
- Song, Y. and Ermon, S. Generative modeling by estimating gradients of the data distribution. *Advances in neural information processing systems*, 32, 2019.

- Song, Y. and Ermon, S. Improved techniques for training score-based generative models. *Advances in neural information processing systems*, 33:12438–12448, 2020.
- Song, Y., Sohl-Dickstein, J., Kingma, D. P., Kumar, A., Ermon, S., and Poole, B. Score-based generative modeling through stochastic differential equations. *arXiv preprint arXiv:2011.13456*, 2020c.
- Song, Y., Durkan, C., Murray, I., and Ermon, S. Maximum likelihood training of score-based diffusion models. *Advances in Neural Information Processing Systems*, 34: 1415–1428, 2021.
- Song, Y., Dhariwal, P., Chen, M., and Sutskever, I. Consistency models. *arXiv preprint arXiv:2303.01469*, 2023.
- Vincent, P. A connection between score matching and denoising autoencoders. *Neural computation*, 23(7):1661–1674, 2011.
- Wang, Z., Lu, C., Wang, Y., Bao, F., Li, C., Su, H., and Zhu, J. Prolificdreamer: High-fidelity and diverse text-to-3d generation with variational score distillation. *Advances in Neural Information Processing Systems*, 36, 2024.
- Xiao, Z., Kreis, K., and Vahdat, A. Tackling the generative learning trilemma with denoising diffusion gans. In *International Conference on Learning Representations*, 2021.
- Xu, Y., Deng, M., Cheng, X., Tian, Y., Liu, Z., and Jaakkola, T. Restart sampling for improving generative processes. *arXiv preprint arXiv:2306.14878*, 2023a.
- Xu, Y., Zhao, Y., Xiao, Z., and Hou, T. Ufogen: You forward once large scale text-to-image generation via diffusion gans. *arXiv preprint arXiv:2311.09257*, 2023b.
- Yin, T., Gharbi, M., Zhang, R., Shechtman, E., Durand, F., Freeman, W. T., and Park, T. One-step diffusion with distribution matching distillation. *CVPR*, 2024.
- Zhang, Q. and Chen, Y. Fast sampling of diffusion models with exponential integrator. In *The Eleventh International Conference on Learning Representations*, 2022.
- Zhang, R., Isola, P., Efros, A. A., Shechtman, E., and Wang, O. The unreasonable effectiveness of deep features as a perceptual metric. In *Proceedings of the IEEE conference on computer vision and pattern recognition*, pp. 586–595, 2018.

A. Theoretical justification for using SDE solvers in CD

Theorem A.1. Let $\Delta t := \max_{n \in [1, N]} |t_{n+1} - t_n|$ where $t \in [\epsilon, T]$. Assume $\mathbf{f}_\theta(\cdot, \cdot)$ is Lipschitz in \mathbf{x} with constant L_1 . Denote $\mathbf{f}(\cdot, \cdot)$ the consistency function of the reverse SDE defined in Equation 3 in the main part of our paper. Assume the SDE solver Φ_{SDE} has a local error bound of $O((t_{n+1} - t_n)^{p+1})$ with $p \geq 1$. Then, if we have $\mathcal{L}_{\mathcal{KL}}^N(\theta, \Phi_{SDE}) = 0$, we have

$$\sup_{n, \mathbf{x}} \|\mathbf{f}_\theta(\mathbf{x}_{t_n}, t_n) - \mathbf{f}(\mathbf{x}_{t_n}, t_n)\|_2 = O((\Delta t)^p).$$

The following lemma provides the convergence proof of using ODE solvers in CD (proof in (Song et al., 2023)), which is crucial to our proof for Theorem A.1.

Lemma A.2 (Proof in (Song et al., 2023)). Let $\Delta t := \max_{n \in [1, N]} |t_{n+1} - t_n|$ where $t \in [\epsilon, T]$. Assume $\mathbf{f}_\theta(\cdot, \cdot)$ is Lipschitz in \mathbf{x} with constant L_1 . Denote $\mathbf{f}(\cdot, \cdot)$ the consistency function of the PF ODE. Assume the ODE solver Φ_{ODE} has a local error bound of $O((t_{n+1} - t_n)^{p+1})$ with $p \geq 1$. Then, if we have $\mathcal{L}_{CD}^N(\theta, \Phi_{ODE}) = 0$, then

$$\sup_{n, \mathbf{x}} \|\mathbf{f}_\theta(\mathbf{x}_{t_n}, t_n) - \mathbf{f}(\mathbf{x}_{t_n}, t_n)\|_2 = O((\Delta t)^p).$$

Proof of Lemma A.2 in (Song et al., 2023). From $\mathcal{L}_{CD}^N(\theta, \Phi_{ODE}) = 0$, derive

$$\mathbf{f}_\theta(\mathbf{x}_{t_{n+1}}, t_{n+1}) \equiv \mathbf{f}(\hat{\mathbf{x}}_{t_n}^{\Phi_{ODE}}, t_n).$$

Denote

$$\begin{aligned} \mathbf{e}_{n+1} &= \mathbf{f}_\theta(\mathbf{x}_{t_{n+1}}, t_{n+1}) - \mathbf{f}(\mathbf{x}_{t_{n+1}}, t_{n+1}) \\ &= \mathbf{f}(\hat{\mathbf{x}}_{t_n}^{\Phi_{ODE}}, t_n) - \mathbf{f}_\theta(\mathbf{x}_{t_n}, t_n) + \mathbf{f}_\theta(\mathbf{x}_{t_n}, t_n) - \mathbf{f}(\mathbf{x}_{t_{n+1}}, t_{n+1}) \\ &= \mathbf{f}(\hat{\mathbf{x}}_{t_n}^{\Phi_{ODE}}, t_n) - \mathbf{f}_\theta(\mathbf{x}_{t_n}, t_n) + \mathbf{f}_\theta(\mathbf{x}_{t_n}, t_n) - \mathbf{f}(\mathbf{x}_{t_n}, t_n) \\ &= \mathbf{f}(\hat{\mathbf{x}}_{t_n}^{\Phi_{ODE}}, t_n) - \mathbf{f}_\theta(\mathbf{x}_{t_n}, t_n) + \mathbf{e}_n, \end{aligned}$$

Recall that $\mathbf{f}_\theta(\cdot, \cdot)$ has Lipschitz constant L_1 ,

$$\begin{aligned} \|e_{n+1}\|_2 &\leq \|e_n\|_2 + L_1 \|\hat{\mathbf{x}}_{t_n}^{\Phi_{ODE}} - \mathbf{x}_{t_n}\|_2 \\ &= \|e_n\|_2 + L_1 \cdot O((t_{n+1} - t_n)^{p+1}) \\ &= \|e_n\|_2 + O((t_{n+1} - t_n)^{p+1}). \end{aligned}$$

With the boundary condition where

$$\mathbf{e}_1 = \mathbf{f}_\theta(\mathbf{x}_{t_1}, t_1) - \mathbf{f}(\mathbf{x}_{t_1}, t_1) = \mathbf{x}_{t_1} - \mathbf{x}_{t_1} = 0,$$

then

$$\begin{aligned} \|e_n\| &\leq \|e_1\| + \sum_{i=1}^{i=n-1} O((t_{i+1} - t_i)^{p+1}) \\ &\leq O(\Delta t^p)(T - \epsilon) = O(\Delta t^p). \end{aligned}$$

With this, the proof for Lemma A.2 is completed. \square

Then we provide the proof for convergence of using SDE solvers in CD.

Proof of Theorem A.1. Consider the reverse SDE,

$$\text{SDE:} \quad d\mathbf{x}_t = [f_t \mathbf{x}_t + \frac{g_t^2}{\sigma_t} \epsilon_\theta(\mathbf{x}_t, t)] dt + g_t d\bar{\mathbf{w}}_t \quad (9)$$

Following (Lu et al., 2022b), we reparameterize the SDE with $\lambda_t = \log \frac{\alpha_t}{\sigma_t}$, $g_t^2 := \frac{d\sigma_t^2}{dt} - 2\frac{d\log\alpha_t}{dt}\sigma_t^2 = -2\sigma_t^2 \frac{d\lambda_t}{dt}$ and $g_t = \sigma_t \sqrt{-2\frac{d\lambda_t}{dt}}$, $d\mathbf{w}_\lambda := \sqrt{-\frac{d\lambda_t}{dt}} d\bar{\mathbf{w}}_t$.

Deriving the integration of Equation (9) from \mathbf{x}_{t_n} to \mathbf{x}_{t_m} ,

$$\mathbf{x}_{t_m} = \underbrace{\frac{\alpha_{t_m}}{\alpha_{t_n}} \mathbf{x}_{t_n}}_{(1)} - \underbrace{2\alpha_{t_m} \int_{\lambda_{t_n}}^{\lambda_{t_m}} e^{-\lambda} \epsilon_\theta(\mathbf{x}_\lambda, \lambda) d\lambda}_{(2)} + \underbrace{\sigma_{t_n} \sqrt{e^{2(\lambda_{t_m} - \lambda_{t_n})} - 1} \mathbf{z}_{t_n}}_{(3)} \quad (10)$$

where $\mathbf{z}_{t_n} \sim \mathcal{N}(\mathbf{0}, \mathbf{I})$. The first-order DPM SDE solver takes the form of

$$\hat{\mathbf{x}}_{t_m}^{\Phi_{\text{SDE}}} = \underbrace{\frac{\alpha_{t_m}}{\alpha_{t_n}} \mathbf{x}_{t_n}}_{(1)} - \underbrace{2\sigma_{t_m} (e^{\lambda_{t_m} - \lambda_{t_n}} - 1) \epsilon_\theta(\mathbf{x}_{t_n}, t_n)}_{(2)} + \underbrace{\sigma_{t_n} \sqrt{e^{2(\lambda_{t_m} - \lambda_{t_n})} - 1} \mathbf{z}_{t_n}}_{(3)} \quad (11)$$

Thus we can bound the local error between Equation (11) and Equation (10). Since the (1) term can be calculated exactly, the total errors Δ between Equation (11) and Equation (10) can be divided into the errors Δ_2 in (2) term and the errors Δ_3 in (3) term

$$\|\mathbf{x}_{t_m} - \hat{\mathbf{x}}_{t_m}^{\Phi_{\text{SDE}}}\|_2 = \|\Delta\|_2 = \|\Delta_2 + \Delta_3\|_2 \leq \|\Delta_2\|_2 + \|\Delta_3\|_2. \quad (12)$$

Denote $h_{t_n} := \lambda_{t_m} - \lambda_{t_n}$ and $\Delta_h := \max_{n \in [1, N]} h_{t_n}$. Consider the $\|\Delta_2\|$ term, we can estimate the error Δ_2 by the Peano remainder term of the Taylor expansion,

$$\int_{\lambda_{t_n}}^{\lambda_{t_m}} e^{-\lambda} \epsilon_\theta(\mathbf{x}_\lambda, \lambda) d\lambda = (e^{-\lambda_{t_n}} - e^{-\lambda_{t_m}}) \epsilon_\theta(\mathbf{x}_{t_n}, t_n) + O((h_{t_n})^2). \quad (13)$$

With this, $\|\Delta_2\|_2$ is bounded by $O((\Delta_h)^2)$.

Consider the $\|\Delta_3\|$ term, we can rewrite

$$\Delta_3 = \sigma_{t_n} \sqrt{e^{2h_{t_n}} - 1} \mathbf{z}_{t_n} - \sigma_{t_m} \sqrt{e^{2h_{t_n}} - 1} \mathbf{z}_{t_m} \quad (14)$$

$$= \frac{\sigma_{t_n}}{t_n} \sqrt{e^{2h_{t_n}} - 1} t_n \mathbf{z}_{t_n} - \frac{\sigma_{t_n}}{t_m} \sqrt{e^{2h_{t_n}} - 1} t_m \mathbf{z}_{t_m}. \quad (15)$$

Since $\lim_{h \rightarrow 0} \frac{\sqrt{e^{2h} - 1}}{h} = 1$, we can derive that

$$\left| \frac{\sigma_{t_n}}{t_n} \sqrt{e^{2h_{t_n}} - 1} - \frac{\sigma_{t_n}}{t_m} \sqrt{e^{2h_{t_n}} - 1} \right| = \left| \frac{\sigma_{t_n}}{t_n t_m} \underbrace{\sqrt{e^{2h_{t_n}} - 1}}_{O(h_{t_n})} \underbrace{(t_n - t_m)}_{O(h_{t_n})} \right|, \quad (16)$$

which is bounded by $O((\Delta_h)^2)$.

Thus, we can derive the bound of the $\|\Delta_3\|$ term,

$$|\Delta_3| = \left| \frac{\sigma_{t_n}}{t_n} \sqrt{e^{2h_{t_n}} - 1} t_n \mathbf{z}_{t_n} - \frac{\sigma_{t_n}}{t_m} \sqrt{e^{2h_{t_n}} - 1} t_m \mathbf{z}_{t_m} \right| \quad (17)$$

$$= \left| \frac{\sigma_{t_n}}{t_n} \sqrt{e^{2h_{t_n}} - 1} t_n \mathbf{z}_{t_n} - \frac{\sigma_{t_n}}{t_m} \sqrt{e^{2h_{t_n}} - 1} t_n \mathbf{z}_{t_n} + \frac{\sigma_{t_n}}{t_m} \sqrt{e^{2h_{t_n}} - 1} t_n \mathbf{z}_{t_n} - \frac{\sigma_{t_n}}{t_m} \sqrt{e^{2h_{t_n}} - 1} t_m \mathbf{z}_{t_m} \right| \quad (18)$$

$$\leq \left| \frac{\sigma_{t_n}}{t_n} \sqrt{e^{2h_{t_n}} - 1} - \frac{\sigma_{t_n}}{t_m} \sqrt{e^{2h_{t_n}} - 1} \right| \cdot |t_n \mathbf{z}_{t_n}| + \left| \frac{\sigma_{t_n}}{t_m} \sqrt{e^{2h_{t_n}} - 1} \right| \cdot |t_n \mathbf{z}_{t_n} - t_m \mathbf{z}_{t_m}|. \quad (19)$$

Notice that $t\mathbf{z}$ is a Wiener process, therefore, we have $|t_n \mathbf{z}_{t_n} - t_m \mathbf{z}_{t_m}|$ bounded by $|O(h_{t_n})|$.

Thus, we have

$$|\Delta_3| \leq \underbrace{\left| \frac{\sigma_{t_n}}{t_n} \sqrt{e^{2h_{t_n}} - 1} - \frac{\sigma_{t_n}}{t_m} \sqrt{e^{2h_{t_n}} - 1} \right|}_{O((h_{t_n})^2) \text{ by Equation (16)}} \cdot \underbrace{|t_n \mathbf{z}_{t_n}|}_{\text{Bounded Random Variable}} + \underbrace{\left| \frac{\sigma_{t_n}}{t_m} \sqrt{e^{2h_{t_n}} - 1} \right|}_{O(h_{t_n})} \cdot \underbrace{|t_n \mathbf{z}_{t_n} - t_m \mathbf{z}_{t_m}|}_{O(h_{t_n})} \quad (20)$$

$$\leq O((h_{t_n})^2) \quad (21)$$

With this, we prove that both $\|\Delta_2\|_2$ and $\|\Delta_3\|_2$ are bounded by $O((\Delta_h)^2)$. Thus we can verify the bound $O((\Delta_h)^2)$ of the total local errors $\|\Delta\|_2$ in Equation (12).

By Lemma A.2, the SDE solver has a local error bound $O((\Delta_h)^2)$, and $O((\Delta_h)^2) = O((\Delta_t)^2)$, we have $\sup_{n, \mathbf{x}} \|\mathbf{f}_\theta(\mathbf{x}_{t_n}, t_n) - \mathbf{f}(\mathbf{x}_{t_n}, t_n)\|_2 = O((\Delta t)^p)$, $p=1$, which completes the proof. \square

B. Multi-step Sampling of Stochastic Consistency Distillation Model

We present the multi-step sampling algorithm of SCott. SCott can generate samples from initial Gaussian noise with one step. As a consistency model, SCott enjoys improving outcomes by alternating denoising and noise injection at inference time. Specifically, at the n -th iteration, we first inject noise to the previous predicting sample \mathbf{z} according to the forward diffusion $\hat{\mathbf{z}}_{t_n} \sim \mathcal{N}(\alpha(t_n)\mathbf{z}, \sigma(t_n)\mathbf{I})$. Then we predict the next \mathbf{z} using SCott. Such a procedure can improve sample quality. Note that $\bar{\mathbf{f}}_\theta$ denotes the function that produces Gaussian mean with the model \mathbf{f}_θ . The pseudo-code is provided in Algorithm 2.

Algorithm 2 Multi-step Stochastic Consistency Model Sampling.

Input: SCott model \mathbf{f}_θ , sequence of timesteps $t_1 > t_2 > t_3 > \dots > t_{N-1}$, noise schedule α_t, σ_t , CFG scale ω , text condition c , initial noise $\hat{\mathbf{z}}_T$
 $\mathbf{z} \leftarrow \bar{\mathbf{f}}_\theta(\hat{\mathbf{z}}_T, c, \omega, T)$
for $n = 1$ to $N - 1$ **do**
 Sample $\hat{\mathbf{z}}_{t_n} \sim \mathcal{N}(\alpha(t_n)\mathbf{z}, \sigma(t_n)\mathbf{I})$
 Sample $\mathbf{z} \leftarrow \bar{\mathbf{f}}_\theta(\hat{\mathbf{z}}_{t_n}, c, \omega, t_n)$
end for
Output: \mathbf{z}

C. Implementation Details

Trainig. We use LAION-Aesthetics- 6+ subset of LAION-5B (Schuhmann et al., 2022) to train our model. We train the model with 4 A100 GPUs and a batch size of 40 for 40,000 iterations. For SD training, the learning rate is 8e-6, and the learning rate is 2e-5 when training discriminator.

Model. We use the publicly available Realistic-Vision-v51 (RV5.1) as the teacher, which is obtained by fine-tuning the pre-trained Stable Diffusion-V1.5 (SD1.5) (Rombach et al., 2022). Both the student and discriminator backbone are initialized by the teacher. When compared to other methods, we use SD1.5 as the teacher for fair comparison. Besides, we apply EMA with a coefficient of 0.995 for the student model.

Table 10. Comparisons with the state-of-the-art methods on MSCOCO-2017 5K in terms of FID, CS, CR. All models are based on DS-V7.

METHOD	STEP	TIME (S)	FID ↓	CS ↑	CR ↑
DPM++ (LU ET AL., 2022B)	25	0.88	31.1	0.325	0.8564
DDIM (SONG ET AL., 2020B)	50	–	32.0	0.323	0.8435
LCM (LUO ET AL., 2023A)	4	0.21	41.1	0.300	0.7495
INSTAFLOW-0.9B (LIU ET AL., 2023)	1	0.09	24.9	0.310	0.8630
SCOTT (OURS)	2	0.13	28.6	0.318	0.8688

D. Additional Results

D.1. Qualitative Results For Table 2 in the main part of our paper

We provide qualitative examples to benchmark our SCott against the state-of-the-art fast sampling methods, LCM (Luo et al., 2023a), InstaFlow (Liu et al., 2023), and DDIM (Song et al., 2020a), DPM++ (Lu et al., 2022b) baselines in Figure 5, corresponding to Table 2 in the main part of our paper.

D.2. Comparison on MSCOCO-2017 5K with Dreamshaper-v7.

InstaFlow and LCM teams release the checkpoints and inference codes of InstaFlow+dreamshaper-7⁴ and LCM-dreamshaper-7⁵, both of which are build on dreamshaper-v7 (DS-V7)⁶. Therefore, we conduct further comparative analysis with LCM and InstaFlow based on DS-V7. Table 10 lists the metrics of different methods evaluated on MSCOCO-2017 5K. We observe our method surpasses InstaFlow-0.9B and LCM with respect to CS and CR, which again indicates our method has better text-to-image consistency and diversity.

For FID, InstaFlow-0.9B (Liu et al., 2023) shows lower value than DPM++ (Lu et al., 2022b), DDIM (Song et al., 2020b) and our method. The probable reason is that zero-shot FID calculated on MSCOCO-2017 5K for evaluating visual quality might not be the most reliable, as discussed in prior works (Betzalel et al., 2022; Podell et al., 2023). Therefore, we exploit qualitative assessment for intuitive comparisons. Figure 6 demonstrates SCott’s generated images are superior to InstaFlow and LCM by a substantial margin. More comparison results are shown in Appendix D.6.

D.3. More Ablation Studies

Table 11. Performance comparison of our SCott on MSCOCO-2017 5K using different teachers with 2-step inference.

TEACHER	FID ↓	CS ↑	CR ↑
SD1.5	22.1	0.308	0.9169
DS-V7	28.6	0.318	0.8688
RV5.1	26.2	0.323	0.8912

Teacher type. Table 11 shows the ablation study on different teacher types. RV5.1 gets the highest CS value, indicating it achieves the highest text-to-image alignment. SD1.5 shows better FID than RV5.1 and DS-V7. This might be because RV5.1 and DS-V7 are fine-tuned from SD1.5 with high-quality images, losing some diversities.

D.4. Visual Results of Diversity

The diversity advantages of our SCott are visualized in Figures 7 to 10. SCott (w/o GAN) denotes the model trained by loss $\mathcal{L}_{\mathcal{KL}}$ while CD is obtained by replacing the SDE solver in SCott (w/o GAN) to ODE solver DDIM. Both the models are initialized by RV5.1. All images are generated with 6 sampling steps. We can observe that SCott (w/o GAN) exhibits more inter-sample diversities. Besides, the SCott (w/o GAN)’s synthesized images present richer details. Generally, SCott (w/o GAN) leads to better human preference than CD.

D.5. Inference steps

As a CM, SCott can improve sample quality as NFE increases. We provide visual results of SCott at inference steps 2, 4, and 8 in Figure 11. The seeds are the same within the columns. SCott can already generate high-quality samples with 2-step inference. With additional steps, SCott can consistently refine the details of the samples.

D.6. Additional Visual Results

Figures 12 to 16 provide more visual results generated by InstaFlow-0.9B, LCM, and our SCott.

⁴<https://github.com/gnabitab/InstaFlow?tab=readme-ov-file>.

⁵<https://huggingface.co/latent-consistency/lcm-lora-sdv1-5>.

⁶<https://huggingface.co/stablediffusionapi/dreamshaper-v7>.

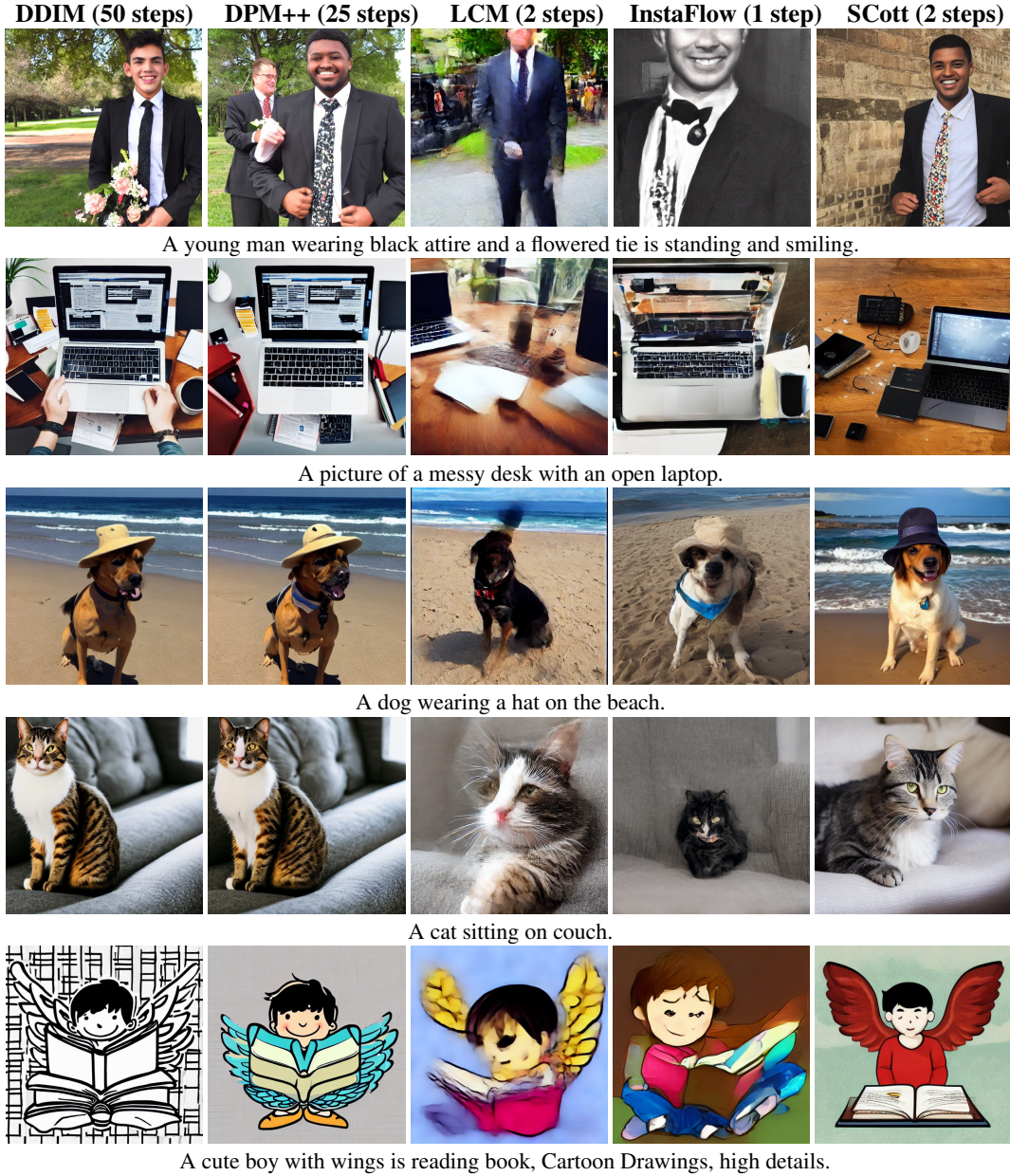


Figure 5. Qualitative comparisons of SCott against competing methods and DDIM, DPM++ baselines. All models are initialized by SD1.5.

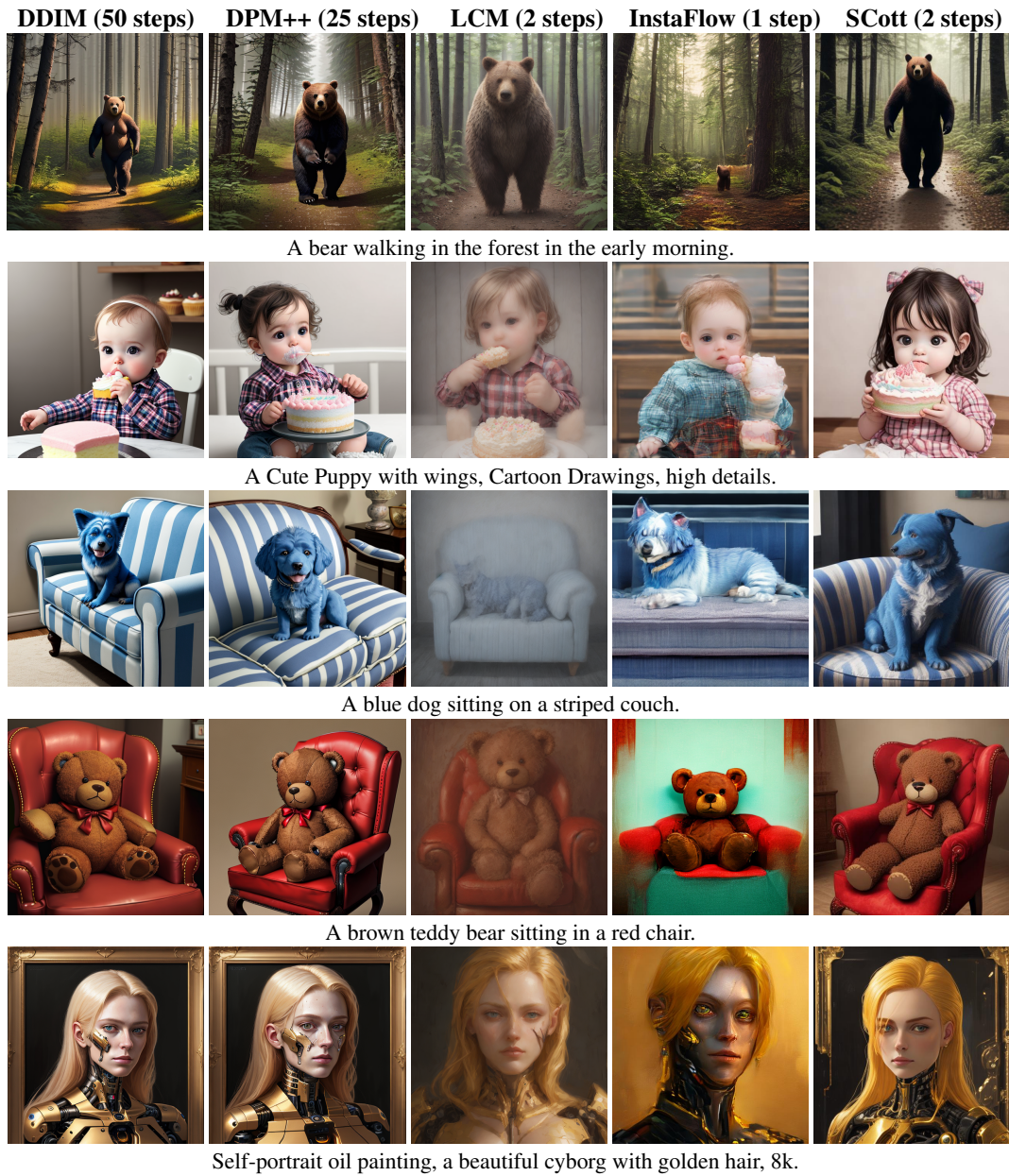


Figure 6. Qualitative comparisons of SCott against competing methods and DDIM, DPM++ baselines. All models are initialized by DS-V7.



Figure 7. Prompt: 2 american bullies with ungre face red eyes crop ears big hed walking torch me.



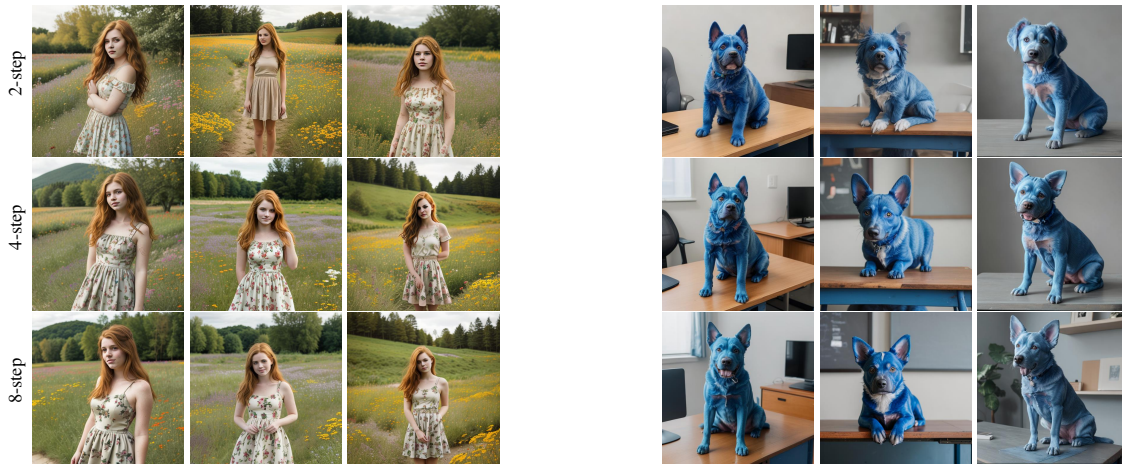
Figure 8. Prompt: A young man wearing black attire and a flowered tie is standing and smiling.



Figure 9. Prompt: A picture of a messy desk with an open laptop.



Figure 10. Prompt: A high-resolution image or illustration of a diverse group of people facing me, each displaying a distinct range of emotions. The image should be in 8K resolution or provide the highest quality available.



”22 year old girl with auburn hair, wearing a skirted dress, very detailed skin texture, drawing on the picture, flowers in the landscape, natural, gentle soul, photojournalism, bokeh.”

”A blue colored dog sitting on a desk.”

Figure 11. Visual results of SCott across inference step 2, 4 and 8. While 2-step SCott can already generate high-quality samples, increasing the inference steps can further refine the details.



InstaFlow (1 step)



LCM (4 steps)



LCM (8-steps)



SCott (2 steps)

Figure 12. Prompt: A small corgi sitting in a movie theater eating popcorn, unreal engine.



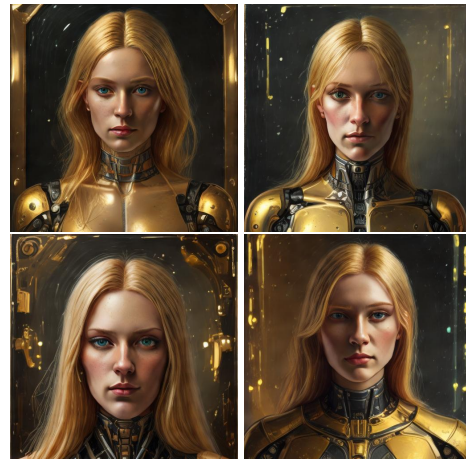
InstaFlow (1 step)



LCM (4 steps)

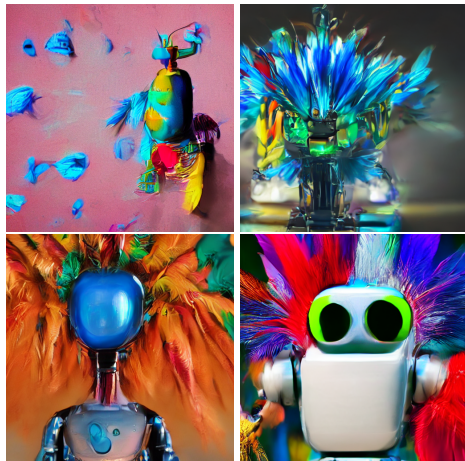


LCM (8-steps)



SCott (2 steps)

Figure 13. Prompt: Self-portrait oil painting, a beautiful cyborg with golden hair, 8k.



InstaFlow (1 step)



LCM (4 steps)



LCM (8-steps)



SCott (2 steps)

Figure 14. Prompt: A cinematic shot of robot with colorful feathers.



InstaFlow (1 step)



LCM (4 steps)



LCM (8-steps)



SCott (2 steps)

Figure 15. Prompt: Hyperrealistic photo of a fox astronaut, perfect face, artstation.



InstaFlow (1 step)



LCM (4 steps)



LCM (8-steps)



SCott (2 steps)

Figure 16. Prompt: A man in a tie and a fake moustache.